Monitoring and Control of Styrene Solution Polymerization Using NIR Spectroscopy

J. M. R. Fontoura, A. F. Santos, F. M. Silva, M. K. Lenzi, E. L. Lima, J. C. Pinto

Programa de Engenharia Química/COPPE, Universidade Federal do Rio de Janeiro, Cidade Universitária, CP: 68502, Rio de Janeiro, 21945-970 RJ, Brasil

Received 10 October 2002; revised 30 December 2002; accepted 30 December 2002

ABSTRACT: Tailored polymer resins are frequently required for a given application. The lack of instruments for in-line monitoring of polymer quality has long been recognized as an important problem in polymerization reactor control. Using the styrene solution polymerization system as an example, we present the use of near-infrared (NIR) spectroscopy as an alternative tool for in-line and *in situ* monitoring and control of monomer conversion and average molecular weight of polymer resins. By using a Kalman filter state estimator and an accurate first-principle model, the control loop could be successfully closed to track desired monomer values and average molecular weights. Two process control strategies, one based on the optimal control theory and the other on model predictive control, were implemented both theoretically and experimentally. The experimental results showed that it is feasible to use NIR spectroscopy for the simultaneous control of monomer conversion and polymer average molecular weight. © 2003 Wiley Periodicals, Inc. J Appl Polym Sci 90: 1273–1289, 2003

Key words: styrene; solution polymerization; NIR spectroscopy; process control; Kalman filter

INTRODUCTION

The polymerization industries work toward increasing production rates of top-quality products at the lowest possible cost while employing the most flexible and safest processes and plant units. This goal is strongly motivated by aggressive commercial competition and an increase not only in the quality expectations of customers but also in the pressure from societal demands for clean plants and chemical processes.[1]

Some of these challenges can be faced with the help of process modeling, control, and optimization techniques. Many successful applications of these techniques on different kinds of polymerization processes have been reported.[2,3] It should be noted that a universal technique, one that can be used in all cases, is not available. Each problem in this field must be carefully analyzed in order to select the most suitable control technique and proper definition of the optimization objectives. To make the best choice, such analysis must take into account such important issues as the complexity of the polymerization reactions, the availability of an accurate mathematical model, and the complexity of the control/optimization objectives.[4]

Correspondence to: J. C. Pinto (pinto@peq.coppe.ufrj.br).

Contract grant sponsors: CAPES and CNPq (Brazilian agencies).

Journal of Applied Polymer Science, Vol. 90, 1273–1289 (2003)

Solution polymerization processes have been widely used for the production of polymer resins. In this process the catalyst, the monomer, and the polymer are all soluble in the reaction media, leading to the formation of a homogeneous reacting mixture. The main disadvantages of solution processes are the low rate of heat removal and the high viscosity of the reaction media when the polymer concentration is large. However, the operation of solution processes is much simpler than the operation of heterogeneous processes. For this reason, reactions can be performed in batch, semicontinuous, and continuous operation modes, and many reactor configurations can be used.[5,6] On the other hand, reaction rates are lower and average molecular weights obtained are smaller when compared to those from bulk and emulsion polymerizations. However, solution reactions can follow step or addition mechanisms.[7]

The main challenges in controlling solution polymerization processes are the control of the average molecular weight,[8] the control of the shape of the molecular weight distribution,[9] the control of the monomer conversion,[5] and the control of the copolymer composition in copolymerizations.[6,10,11] Because of the much simpler reaction operation and the availability of good mathematical models, many works regarding the control of solution polymerization processes can be found in the literature.[3] However, most have reported the results of simulations; none have reported the actual implementation of closed-loop algorithms for the simultaneous control of monomer

conversion and average molecular weight of polymer resin.

Tailored polymer resins are frequently required for a given application. To produce a specific resin, using an efficient control technique may not be enough. The gap between the polymerization process and the control technique must be bridged with accurate and robust instruments for in-line monitoring, so that the controller can know the correct current states of the process. The lack of adequate instrumentation for measuring and monitoring polymer quality has long been recognized as an important problem in polymerization reactor control.[12] Different hardware sensors used in the monitoring of polymerization processes were reviewed by Chien and Penlidis[13] and Kammona et al.[14]

Near-infrared (NIR) spectroscopy has been used successfully to close the control loop in some polymerization processes. It was used to monitor the average particle size in styrene suspension polymerization reactors and to close the loop for particle size control.[15,16] More recently, NIR spectroscopy was used to close the process control loop in an emulsion polymerization reactor in order to obtain polymer resins with a specified composition and average molecular weight.[17] The main advantages of NIR systems are having the feasibility of in-line and *in situ* analyses, avoiding undesirable time delays, and reducing the potentially large experimental error involved with the sample preparation step. The use of NIR spectroscopy for the monitoring and control of solution polymerization reactors is reviewed next.

Long et al.[18] showed that NIR spectroscopy could be utilized to monitor monomer conversion during conventional anionic solution polymerization. The conversion of the vinyl protons in the monomer to methylene protons in the polymer was easily monitored under conventional solution polymerization conditions. The authors investigated styrene and isoprene polymerization kinetics in nonpolar and polar solvents, and relative rate constants were compared to values previously reported in the literature. In addition, copolymerization kinetics also were able to be studied. Preliminary data suggested that NIR spectroscopy could be used to detect the sequence distributions for tapered block copolymers, geometric isomer content, and reactivity ratios for free-radical copolymerization.

The use of NIR spectroscopy to monitor the production of polyurethanes in solution polymerization processes was reported by DeThomas et al.[19] A Beer law model was derived for the quantitative determination of isocyanate concentration in the urethane polymerization reaction. Statistical process control was used to observe trends in the polymerization reaction. The integration of the NIR spectrophotometer directly into the process was able to provide real-time chemical information, yielding significant improvement in product quality and consistency, while minimizing reaction time.

Cherfi et al.[20,21] recently reported on the use of NIR spectroscopy to monitor the monomer conversion and weight-average molecular weight of the polymer produced during solution polymerization of methyl methacrylate (MMA). According to the authors, the NIR spectra were recorded during batch and semicontinuous reactions using an *in situ* transmission probe. Off-line gravimetry and gel permeation chromatography (GPC) were used as reference methods to provide the conversion and average molecular weight data set required for the calibration procedure. Using partial least-squares regression (PLS), an empirical model was built to relate the NIR spectral data to the two polymerization variables of interest. The measurements were then validated for various operating conditions and for both batch and semicontinuous modes. The in-line NIR measurements were thus demonstrated to be robust and accurate.

This article reports on the first use of NIR spectroscopy to simultaneously control solution polymerization and monitor the reactor evolution. The control scheme was implemented both theoretically and experimentally, allowing for the simultaneous control of monomer conversion and average polymer molecular weight in batch free-radical styrene solution polymerization. Initially, reactions were performed in order to allow for the development of an empirical model for in-line conversion monitoring using off-line gravimetrical analysis and the MLR (multiple linear regression) method. Afterward, Kalman filtering techniques were implemented to allow for the estimation of the molecular weight averages using an accurate first-principles model. Once the control loop could be closed, an optimal control technique and the model-based predictive control strategy were applied to the polymerization system in order to control the monomer conversion and the molecular weight averages through manipulation of monomer concentrations, initiator concentrations, and reactor temperature profiles. Very good results were achieved, showing that the NIR system can be used efficiently as in-line and *in situ* instrumentation for the control of solution polymerization reactors.

Theoretical framework

The mathematical model developed and a brief discussion about the process control strategies adopted to monitor the conversion and molecular weight averages are presented here. It must be stressed that our main goal was to study the application of NIR spectroscopy in solution polymerization process control and not to compare the implemented process control and state estimation techniques with alternative available techniques. For this reason, the presentation is as simple and short as possible.

TABLE I
Free-Radical Polymerization Mechanism

Initiation	$I \xrightarrow{k_d} 2R^{\bullet}$
	$R^{\bullet} + M \rightarrow P_1$
Propagation	$P_n + M \xrightarrow{k_p} P_{n+1}$
Chain transfer to monomer	$M + P_m \xrightarrow{k_{fm}} \Theta_m + P_1$
Chain transfer to solvent	$S + P_m \xrightarrow{k_{fs}} \Theta_m + P_1$
Termination by combination	$P_n + P_m \xrightarrow{k_{tc}} \Theta_{n+m}$

Mathematical model for styrene solution free-radical polymerization

A mathematical model, based on the classical free-radical reaction mechanism presented in Table I, was developed to describe the behavior of the batch styrene solution polymerization process.

The following set of mass balance equations can be obtained for initiator, monomer, solvent, growing radicals with chain length n, and dead polymer chains with chain length n, respectively. It was assumed that the reaction is performed at constant temperature, that stirring conditions are ideal, and that kinetic constants are size independent.

$$\frac{dI}{dt} = -k_d \cdot I \tag{1}$$

$$\frac{dM}{dt} = -\frac{(k_p + k_{fm})}{V} \cdot M \cdot \sum_{n=1}^{\infty} P_n \tag{2}$$

$$\frac{dS}{dt} = -\frac{k_{fs}}{V} \cdot S \cdot \sum_{n=1}^{\infty} P_n \tag{3}$$

$$\frac{dP_1}{dt} = 2 \cdot f \cdot k_d \cdot I - \left(\frac{(k_p + k_{fm})}{V} \cdot M + \frac{k_{fs}}{V} \cdot S\right) \cdot P_1 + \left(\frac{k_{fm}}{V} \cdot M + \frac{k_{fs}}{V} \cdot S - \frac{k_{tc}}{V} \cdot P_1\right) \cdot \sum_{n=1}^{\infty} P_n \tag{4}$$

$$\frac{dP_n}{dt} = \frac{k_p}{V} \cdot M \cdot P_{n-1} - \left(\frac{(k_p + k_{fm})}{V} \cdot M + \frac{k_{fs}}{V} \cdot S\right) \cdot P_n - \frac{k_{tc}}{V} \cdot P_1 \cdot \sum_{n=1}^{\infty} P_n \quad n \geq 2 \tag{5}$$

$$\frac{d\theta_n}{dt} = \left(\frac{k_{fm}}{V} \cdot M + \frac{k_{fs}}{V} \cdot S\right) \cdot P_n + \frac{k_{tc}}{2 \cdot V} \cdot \sum_{m=1}^{n-1} P_m \cdot P_{n-m} \tag{6}$$

From eqs. (4–6) the leading moments of the size distributions for the growing radical chains (λ_k) and the dead polymer chains (μ_k) can be easily obtained.[22] It must be emphasized that the leading moments of the molecular weight distributions are sufficient to determine the molecular weight averages but not to provide any conclusive information about the shape of the molecular weight distribution of the polymer resin. The moment equations are presented below:

$$\frac{d\lambda_0}{dt} = 2 \cdot f \cdot k_d \cdot I - \frac{k_{tc}}{V} \cdot (\lambda_0 \cdot \lambda_0) \tag{7}$$

$$\frac{d\lambda_1}{dt} = 2 \cdot f \cdot k_d \cdot I + \frac{k_{tc}}{V} \cdot M \cdot \lambda_0 + \left(\frac{k_{fm}}{V} \cdot M + \frac{k_{fs}}{V} \cdot S\right) \cdot (\lambda_0 - \lambda_1) - \frac{k_{tc}}{V} \cdot (\lambda_0 \cdot \lambda_1) \tag{8}$$

$$\frac{d\lambda_2}{dt} = 2 \cdot f \cdot k_d \cdot I + \frac{k_{tc}}{V} \cdot M \cdot (\lambda_0 + 2 \cdot \lambda_1) + \left(\frac{k_{fm}}{V} \cdot M + \frac{k_{fs}}{V} \cdot S\right) \cdot (\lambda_0 - \lambda_2) - \frac{k_{tc}}{V} \cdot (\lambda_0 \cdot \lambda_2) \tag{9}$$

$$\frac{d\mu_0}{dt} = \left(\frac{k_{fm}}{V} \cdot M + \frac{k_{fs}}{V} \cdot S\right) \cdot \lambda_0 + \frac{k_{tc}}{2 \cdot V} \cdot (\lambda_0 \cdot \lambda_0) \tag{10}$$

$$\frac{d\mu_1}{dt} = \left(\frac{k_{fm}}{V} \cdot M + \frac{k_{fs}}{V} \cdot S\right) \cdot \lambda_1 + \frac{k_{tc}}{V} \cdot (\lambda_1 \cdot \lambda_0) \tag{11}$$

$$\frac{d\mu_2}{dt} = \left(\frac{k_{fm}}{V} \cdot M + \frac{k_{fs}}{V} \cdot S\right) \cdot \lambda_2 + \frac{k_{tc}}{V} \cdot (\lambda_0 \cdot \lambda_2 + \lambda_1 \cdot \lambda_1) \tag{12}$$

The number-average molecular weight (M_n), the weight-average molecular weight (M_w), and the monomer conversion are given by

$$M_n = \frac{\mu_1 + \lambda_1}{\mu_0 + \lambda_0} \cdot PM_{\text{monomer}} \tag{13}$$

$$M_w = \frac{\mu_2 + \lambda_2}{\mu_1 + \lambda_1} \cdot PM_{\text{monomer}} \tag{14}$$

$$X = 1 - \left(\frac{M}{M_0}\right) \tag{15}$$

TABLE II
Model Kinetic Constants and Physical Properties

Parameter	Unit	Reference
$k_d = 7.12 \cdot 10^{13} \cdot e^{[-(29589/R \cdot T)]}$	s^{-1}	BRANDRUP & IMMERGUT (1975)
$k_p = 1.051 \cdot 10^{7} \cdot e^{[-(7060/R \cdot T)]}$	$\frac{L}{mol \cdot s}$	HSU & CHEN (1988)
$k_{tc_0} = 1.255 \cdot 10^{9} \cdot e^{[-(1680/R \cdot T)]}$	$\frac{L}{mol \cdot s}$	HSU & CHEN (1988)
$k_{fm} = 2.31 \cdot 10^{6} \cdot e^{[-(12670/R \cdot T)]}$	$\frac{L}{mol \cdot s}$	HSU & CHEN (1988)
$k_{fs} = 5.92 \cdot 10^{8} \cdot e^{[-(17210/R \cdot T)]}$	$\frac{L}{mol \cdot s}$	HSU & CHEN (1988)
$\varepsilon = 0.1506 + 4.436 \cdot 10^{-4} \cdot (T - 273.15)$	—	SCHULER & ZHANG (1985)
$\rho_m = \frac{1}{0.8075 + 1.0 \cdot 10^{-3} \cdot T}$	$\frac{g}{mL}$	STEVENS (1988)
$\rho_s = \frac{1}{1.047 + 4.9 \cdot 10^{-4} \cdot T}$	$\frac{g}{mL}$	STEVENS (1988)
$f = 0.72$	—	SWERN (1970)
$PM_{monomer} = 114.0$	$\frac{g}{gmol}$	PERRY & GREEN (1997)
$\alpha = 0.5093$	—	CHEN & HUANG (1981)
$\beta = 2.2395$	—	CHEN & HUANG (1981) (adapted)
$\gamma = 3.0943$	—	CHEN & HUANG (1981) (adapted)

Two important phenomena must be taken into account during model formulation. The first is related to the decrease of the volume of the reaction mixture because of the difference between the densities of the monomer and the polymer resin. The total volume of the reaction mixture can be computed as

$$V = V_S + V_{m0} \cdot (1 - \epsilon \cdot X) \tag{16}$$

which considers a linear dependence of the volume with the monomer conversion.[23] Therefore, monomer and polymer densities are assumed to be constant. The second phenomenon is related to the gel effect, which was computed with the empirical equation proposed by Chen and Huang.[24]

$$g = \left(\frac{k_{tc}}{k_{tc_0}}\right)^{0.5} = \alpha + \beta \cdot X + \gamma \cdot X^2 \tag{17}$$

In this case, the original values of α, β, and γ were modified to compensate for changes in solvent concentration. To correct the original parameters, it was assumed that the gel effect depended only on the total polymer concentration, expressed as a mass fraction. These model parameters were validated by Fontoura[25] for monomer conversions between 30% and 80%, with very good model performance. All kinetic constants required for simulations are presented in Table II.

Optimal control

One of the process control strategies used in this work to evaluate the feasibility of NIR spectroscopy as a process monitoring technique was derived from the optimal control theory.[26] The optimal control policy is computed numerically by dividing the total batch time into N time intervals of equal length, according to the procedure developed by Hsu and Chen,[27] as presented in Figure 1.

The strategy consists of obtaining: the amount of initiator that should be added to the reaction system at the beginning of each time interval (b_j); the reactor temperature of each time interval (T_j); the duration of each interval of the reaction (t_j) that would minimize the total batch conversion time of a specified desired value of the monomer (from which M_N can be obtained; Fig. 1); the number-average (or weight-average) molecular weight (from which $\mu_{0,N}$ can be obtained; Fig. 1); and the number of intervals (N). Therefore, the control policy is computed numerically for a minimum batch time problem in which the manipulated variables are the reactor temperature and the initiator concentration, and the polymer properties and final conversion are specified as set-point constraints.

$$\min_{T_j, t_j, b_j} (t = N \cdot t_j)$$

$$Mn(t) = Mn_d$$

$$Mw(t) = Mw_d$$

$$X(t) = X_d$$

$$t_i = t_j;\ i \neq j \tag{18}$$

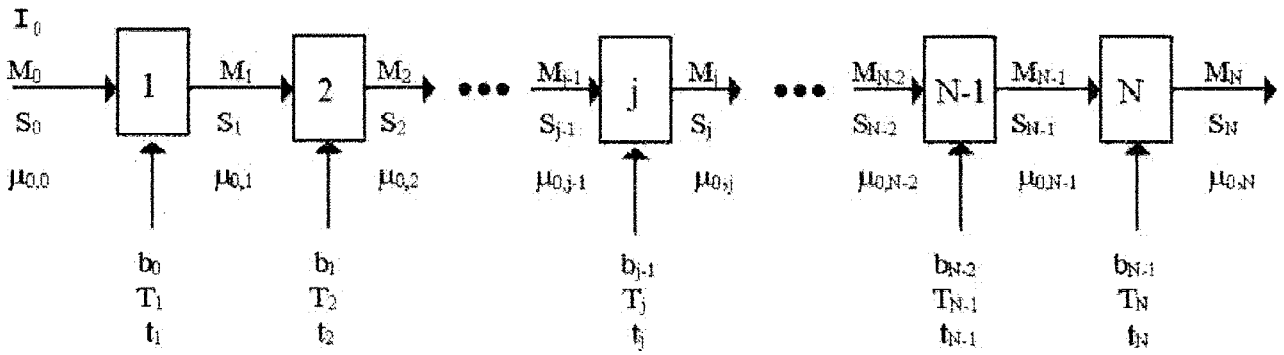

Figure 1 Division of the batch time into *N* intervals.

The model that has been developed, which was explained in an earlier section, is used to calculate how the batch time, the overall monomer conversion, and the polymer properties depend on the reactor temperature and initiator concentration profiles.

It must be noted that although the whole batch is not necessarily carried out at the same temperature, each reaction interval is assumed to be operated under isothermal conditions. This is why an isothermal model can be used for model computations. This can be understood as a zero-order discretization of the time domain. The control policies are then obtained with the help of standard nonlinear optimization algorithms. More details can be obtained in Hsu and Chen[27] and Fontoura.[25]

This technique was used to perform open-loop control and to provide a benchmark for evaluation of the closed-loop control scheme. In this case, optimum theoretical operation policies were previously determined and then implemented experimentally in order to produce a polymer resin with specified properties. The NIR spectroscopy results were used only to provide actual information about the current states of the reactor and afterward to evaluate the performance of the state estimator described below.

Model predictive control

In addition to the discrete optimal control strategy, nonlinear model predictive control also was used to evaluate the feasibility of NIR spectroscopy as an alternative in-line process-monitoring technique. The model predictive control technique is briefly explained here. Further details can be found in Morari and Lee.[28]

The main objective of the model predictive control technique is to determine a set of control actions through the minimization (or maximization) of a specified objective function. The objective function is formulated by assuming that the system should be able to track a desired trajectory in a given control horizon of size M, as presented in Figure 2. After computation of the control actions, only the first calculated control action is actually implemented in the system. By using available instrumentation, some states of the system are measured, and some others are estimated using filtering techniques. After updating the states of the system, the optimization problem is solved again, and the algorithm is repeated iteratively until the specified batch time and/or reactor properties reach the desired values. It must be stressed that some constrains must usually be taken into account during the optimization problem in order to avoid saturation of the valves and to allow for the secure operation of the system.

A general formulation for the optimization problem follows [a given objective function must be minimized (or maximized)]:

$$\min_{u(k),\ldots\mu(k+M-1)} \Theta(u) = \int_{t_k}^{t_k+T_p} [e(t)]^2\, dt$$

$$= \sum_{i=1}^{k+P} [y_{\text{setpoint}}(i) - y_{\text{model}}(i)]^2 \quad (19)$$

which is subject to:

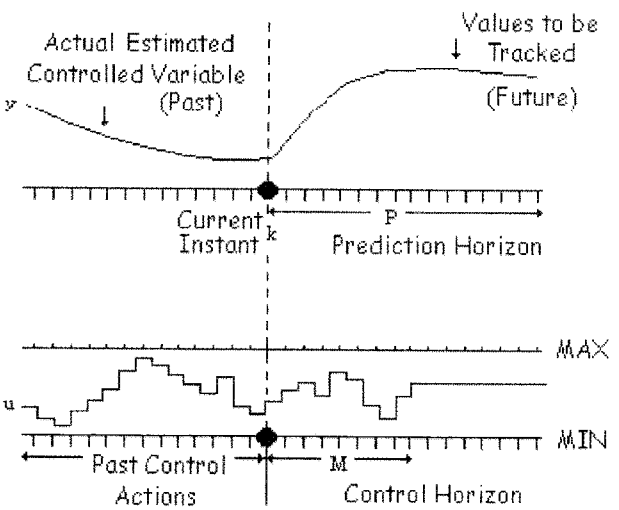

Figure 2 Model predictive control schematic representation.

$$\frac{dx}{dt} = f(x, u) \tag{20}$$

$$y = h(x) \tag{21}$$

$$u_{\min} \le u(i) \le u_{\max} \tag{22}$$

$$u(i-1) - \Delta u_{\max} \le u(i) \le u(i-1) + \Delta u_{\max} \tag{23}$$

$$u(i) = u(k+M-1) \quad \text{for all } i > k+M-1 \tag{24}$$

$$x_{\min} \le x(i) \le x_{\max} \tag{25}$$

$$y_{\min} \le y(i) \le y_{\max} \tag{26}$$

$$x(t_k) = x_k \tag{27}$$

The objective function can include economic, safety, and other process criteria. The dynamics of the system states, which are captured as the output values y, are described in eqs. (20) and (21). An indication that certain system constraints must be satisfied is shown in eqs. (22)–(26). P and M are the prediction and control horizons, respectively, and are varied in order to achieve a better performance of the process controller. Standard nonlinear optimization algorithms can help to minimize eqs. (19)–(27).[28]

Two control strategies were adopted to track the control objectives in the application of the model predictive control technique used in this work. The first strategy was based on manipulation of the amount of initiator added in the reaction system in order to follow specified dynamic profiles for monomer conversion and molecular weight averages. The second strategy was based on manipulation of the temperature at each reaction interval in order to follow a desired monomer conversion profile. M was not pursued in this case. The results obtained with the open-loop optimal control technique were used as reference trajectories for the closed-loop control problem. The control loop was closed with the feedback information from the NIR spectroscopy and the Kalman filter. As shown below, very accurate feedback information about the current states of the polymerization reactor could be provided by the devised monitoring scheme.

State estimation

There are many state estimation techniques available in literature.[29–31] Each technique has its peculiarities and is suitable for a specific process. Because of its simplicity and the characteristics of the mathematical model available for the polymerization process, an extended Kalman filter was used here as the state estimation technique. A detailed mathematical formulation of the extended Kalman filter can be found in many different sources, for example, Kozub and MacGregor.[30]

A general formulation of the Kalman filter takes into consideration that the process model is continuous and that the output model is discrete as

$$\frac{dx}{dt} = f(x, u, t) + w(t) \tag{28}$$

$$y_k = h_k(x(t_k)) + v_k \tag{29}$$

where the process disturbances and experimental errors are $w(t)$ and v_k, respectively, which can be considered noncorrelated, and independent white (Gaussian) noise with zero mean and covariance, given by:

$$E(ww^T) = R_w \tag{30}$$

$$E(wv^T) = 0 \tag{31}$$

$$E(vv^T) = R_v \tag{32}$$

where $E(\bullet)$ is the average operation.

Using eqs. (28)–(32), state estimates can be updated as follows.[30] First, using eqs. (33)–(34), the state $\hat{x}(-)$ and error $P_k(-)$ are predicted with the model equations. Then the filter gain is updated using eq. (35), and the states $\hat{x}(+)$ and error $P_k(+)$ are updated with eqs. (36) and (37) so that the new set of available data is taken into account. An algorithm is applied recursively in order to obtain the reactor states at the desired sampling intervals. In the case analyzed here, the reactor states are presented in eqs. (1)–(12), whereas the output values that were observed by NIR spectrophotometry are described by eq. (15).

$$\frac{d\hat{x}}{dt} = f(\hat{x}, t) \tag{33}$$

$$\frac{dP}{dt} = F(\hat{x}, t) \cdot P(t) + P \cdot F^T(\hat{x}, t) + R_w \tag{34}$$

$$K_k = P_k(-) \cdot H_k^T(\hat{x}(-)) \cdot [H_k(\hat{x}(-)) \cdot P_k(-) \cdot H_k^T(\hat{x}(-)) + R_v]^{-1} \tag{35}$$

$$\hat{x}_k(+) = \hat{x}_k(-) + K_k \cdot [y_k - h_k(\hat{x}_k(-))] \tag{36}$$

$$P_k(+) = [I - K_k(\hat{x}_k(-))] \cdot P_k(-) \tag{37}$$

where

$$F(\hat{x}, t) = \left.\frac{\partial f(x, t)}{\partial x(t_k)}\right|_{x=\hat{x}(t)} \tag{38}$$

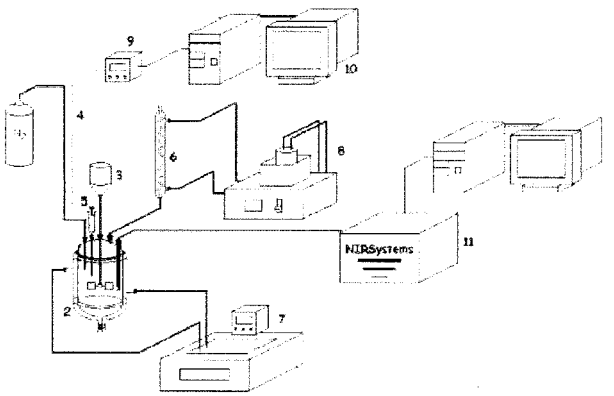

Figure 3 Schematic representation of the experimental setup.

$$H_k(\hat{x}_k(-)) = \left.\frac{\partial h_k(x(t_k))}{\partial x(t_k)}\right|_{x(t_k)=\hat{x}_k(-)} \tag{39}$$

EXPERIMENTAL

Chemicals

For the solution polymerization system, benzoyl peroxide (BPO), with a moisture content of 25%, supplied by Vetec Química Fina (São Paulo, SP, Brazil), was used as initiator. Styrene supplied by Nitriflex Resinas S/A (Rio de Janeiro, RJ, Brazil), with 20 ppm of inhibitor (hydroquinone) and a minimum purity of 99.5% on a mass basis, was used as monomer. Toluene, supplied by Vetec Química Fina (São Paulo, SP, Brazil), less than 1% impure, was used as the reaction media. Distilled water was used as the heat exchange fluid for the reactor jacket. Hydroquinone (Vetec Química Fina, São Paulo, SP, Brazil), less than 1% impure, was used for reaction halting. Nitrogen, supplied by AGA S/A (Rio de Janeiro, RJ, Brazil) and less than 0.01% impure, was used to maintain the inert atmosphere during the polymerizations reactions. Tetrahydrofuran (THF), less than 0.1% impure, was used for gel permeation chromatography, and ethylene glycol was used for refrigeration. Both were supplied by Vetec Química Fina (São Paulo, SP, Brazil). All chemicals were used as received, without further purification.

Reaction system

The experimental setup used to carry out the polymerization reactions is shown in Figure 3. The apparatus used was similar to the one described by Santos et al.[16] The data acquisition system used was similar to the one described by Neitzel and Lenzi,[32] using the LabView® Student version.[33]

The components of the experimental apparatus (Fig. 3) were: a nitrogen cylinder (AGA S/A, Rio de Janeiro, Brazil), (a 1.0-L jacketed glass reactor (FGG Equipamentos Cientificos, LTDA, São Paulo, Brazil), a mechanical agitator (Fisatom 713-T, São Paulo, Brazil) equipped with a six-blade impeller, a J-type thermocouple (Ecil, São Paulo, Brazil), a syringe (Omega, São Paulo, Brazil), for sample collecting, a condenser to avoid monomer loss, a thermostatic bath (Haake DC-3, Paramus, NJ) for the reactor jacket, a refrigerator bath (PolyScience KR30-A, Niles, IL) for the condenser, a National Instruments SCXI-1000 chassis (Austin, TX) for signal conditioning, a microcomputer (Pentium MMX 233 MHz, Santa Clara, CA) for data acquisition, and an NIR spectrophotometer (NIRSystem 6500, Silver Springs, MD). Additional details are provided in Santos et al.[16]

Product characterization

Monomer conversion measurements were obtained by gravimetrical analysis, with the polymer samples dried in a recirculation oven at 45°C until they were a constant weight. Finally, molecular weight average and molecular weight distribution values were obtained with a gel permeation chromatograph. The system was composed of three linear columns (Phenomenex), with gel porosity ranging from 10^3 to 10^6 Å. Calibration was done with polystyrene standards (Phenomenex) whose molecular weights ranged from 10^4 to 2.0×10^6. THF was used as the mobile phase, and the analysis was carried out at 40°C. The refractive index detector (SFD: RI-2000F) and the pumping system (Konik) were connected to a Pentium MMX 233 MHz microcomputer for data acquisition and data handling.

Experimental procedure

Before the reactor charge, the system was purged with nitrogen to maintain the inert atmosphere. The specific amounts of monomer (styrene) and solvent (toluene) previously weighed were then added to the reactor, and the heating system was turned on to reach the desired start-up temperature. The reaction mixture was kept strongly agitated. After reaching the nominal temperature, the initiator (BPO) was fed to the system as a concentrated toluene solution, and, simultaneously, NIR spectroscopy was used to monitor the process. During the experimental runs 3.0-mL samples were withdrawn along the reaction course using a 10.0-mL glass syringe. Samples were added to a previously weighed flask containing 2.0 mg of hydroquinone solution at a rate of 2.0 g/L for reaction halting.

The experimental runs were divided into four groups. The first group was composed of reactions for building a model to evaluate the feasibility of NIR spectroscopy as a useful monomer conversion monitoring technique. The reactions were carried out at a temperature of 90°C with a solid content of 70 wt %.

The second group consisted of reactions for validating the developed model with additional, independent experimental results. The third group was composed of experimental runs involving the use of open-loop optimal control techniques for control purposes, and the last group comprised experiments in which model predictive control techniques were used to monitor and control the properties of the polymer resins.

In all experiments the maximum solid content was made equal to 70 wt %, in accordance with actual industrial solution polymerization processes. Monomer conversion was varied from 0% to 85%, so that polymer concentration would sometimes be as high as 60 wt %. Note that despite the high solution viscosities reached in certain experiments, monitoring and control procedures never failed. This is very important because alternative monitoring techniques, such as densimetry and refractometry, would probably require the installation of a sampling circuit and a lower solid content to avoid plugging inside the recirculation lines. This can be considered a clear indication of the adequacy of the NIRS-based monitoring and control procedures.

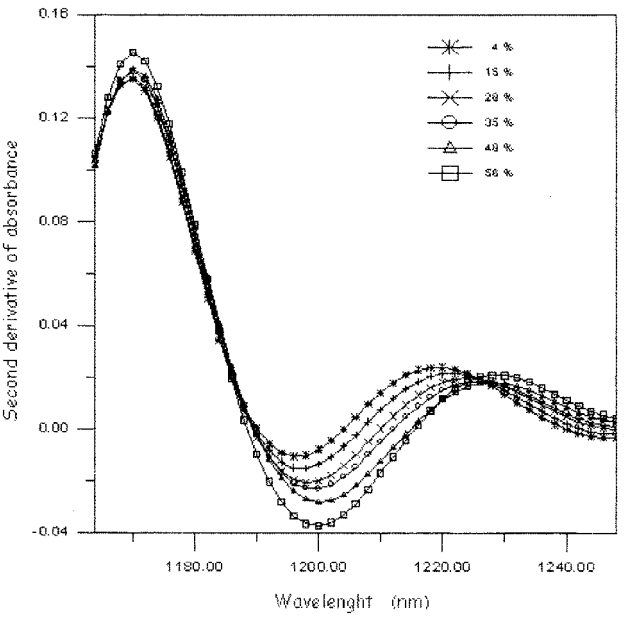

Figure 5 Evolution of second derivative spectra of polystyrene in a solution polymerization reaction.

RESULTS AND DISCUSSION

Feasibility of NIR spectroscopy monitoring

The successful use of NIR spectroscopy for process monitoring and control resulted not only from the in-line and *in situ* measuring capabilities[34] but also from the development of accurate and easy-to-use chemometric techniques.[35] The literature has additional details and information about the theory of NIR spectroscopy[36,37] and spectroscopical device design and software analysis systems.[34]

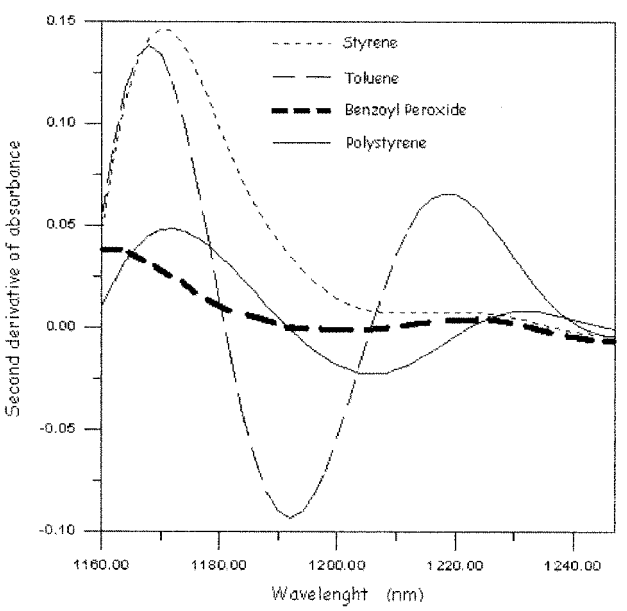

Figure 4 Second derivative spectra of styrene, polystyrene, toluene, and benzoyl peroxide in the region of 1150–1240 nm.

The first step toward the development of a calibration model for NIR spectroscopy consisted of analyzing the spectra of the constituents of the reaction media. This was done to check for the existence of spectral regions where it would be possible to differentiate the absorption signals of the various components, so those component concentrations could be quantified. Treating the NIR spectra should lead to better results.[15] The most common approach is to work with the spectra of the second derivative of absorbance, as it eliminates base line differences and provides better spectral resolution.

Analyzing the spectra of the second derivative of absorbance for the components of the reaction mixture allows attention to be focused in the region of 1150–1240 nm, characterized by the absorption band of the second overtones of the bonds CH and CH_2. In this region, as can be seen in Figure 4, the polystyrene spectrum had a minimum at 1207 nm, whereas styrene and benzoyl peroxide did not show significant absorption. Although the toluene spectrum had a minimum at 1192 nm, the toluene composition did not change, so that this region could be used for purposes of this study. Once the region of analysis was determined, solution polymerization reactions were carried out to obtain experimental data for model building. Figure 5 shows the evolution of the second derivative spectra of the reaction medium during a particular experimental run.

Using the MLR (multiple linear regression) calibration technique,[34] a simple but very accurate model

was derived to monitor the monomer conversion. The model, given by eq. (40), actually used the second derivative absorbance at 1207 nm to yield the weight fraction of polystyrene present in the reaction media and showed a correlation coefficient (R^2) of 0.99. The model was derived using 15 samples obtained from three experimental runs in which the maximum solid content was 70% and monomer conversions ranged from 0% to 60%.

$$PSt = 19.48 - 1606.0 \cdot A_{\lambda=1207\ \mathrm{nm}} \qquad (40)$$

Figure 6 shows a comparison of off-line (gravimetry) and in-line (NIR spectroscopy) values of the weight fraction of polystyrene for the data set used for model derivation. A very good correlation between both data sets can be observed.

A second group of reactions was carried out to validate the NIR model given by eq. (39). This group comprised six experimental runs whose maximum solid content was 70% and whose monomer conversions ranged from 10% to 60%. Figure 7 presents a comparison of the in-line values, predicted by eq. (39), and the off-line data. Excellent agreement between data can also be observed, validating the proposed model.

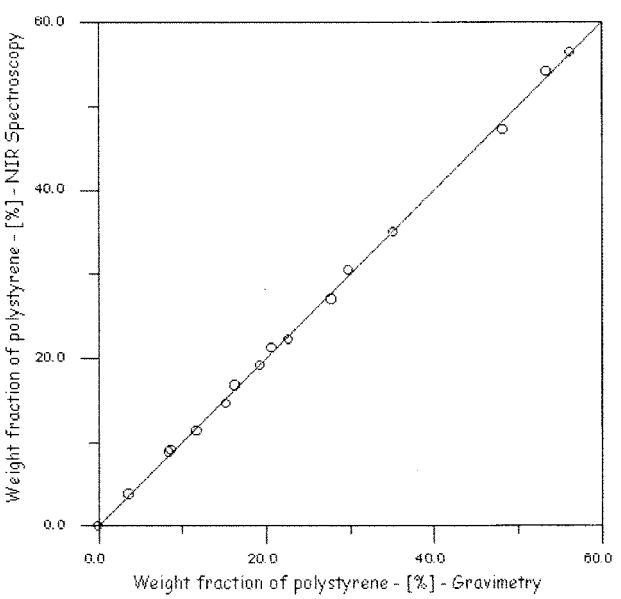

Figure 6 Comparison of off-line (gravimetry) and in-line (NIR spectroscopy) values of the weight fraction of polystyrene.

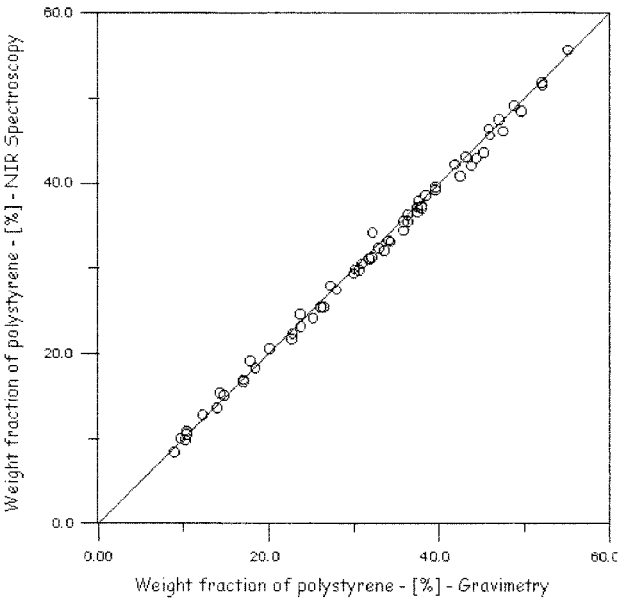

Figure 7 Validation of the NIR spectroscopy model for monomer conversion monitoring with independent experimental data.

Process control experiment

Through the study presented in the previous section a new tool became available for successful in-line and *in situ* monomer conversion monitoring. A simple but very accurate model allowed for the determination of the weight fraction of polystyrene in the reaction media. In addition, this tool presents new opportunities in polymerization process control because it can be used to close the loop control and provide feedback information about the current states of the reactor. To evaluate the use of this new tool, two process control strategies were implemented to monitor and control monomer conversion and polymer average molecular weight. It must be noted that controlling the value of M_n is similar to controlling the value of M_w because the polydispersity index varies very little in styrene solution reactions. For this reason, control objectives can be described in terms of either M_n or M_w, although it is well known that experimental values of M_w are more precise and, for this reason, normally used for control purposes. Initiator additions were performed through fast feeding of known amounts of the initiator solution, and temperature manipulations were performed through the manipulation of the set-point temperature of the thermostatic bath.

Optimal control

One of the strategies adopted was derived from the optimal control theory, as explained above, on optimal control. Because of the time delay of the thermostatic bath, the temperature of the system was kept constant at specified values during the first experimental runs. Therefore, additional constraints were defined, as presented in eq. (18). The experimental runs were designed to evaluate the influence of the number of intervals used to discretize the batch. The desired set-point values of the final monomer conversion and

TABLE III
Set-Point Values and Experimental Results of Optimal Control-Based Technique

Exp.	X_d	M_{n_d}	X_{exp}	$M_{n_{\text{exp}}}$	N	$[I]_0 \cdot 10^2$ (mol/L)	$[b_i] \cdot 10^2$ (mol/L)	t_f (h)	T (°C)
1	0.64	54500	0.60	52922	1	0.9070	0	7.00	91
2	0.78	45000	0.72	49337	1	1.3381	0	8.00	91
3	0.44	82400	0.40	88704	1	0.4894	0	6.85	85
4	0.44	82400	0.41	104067	4	0.3023	0.1008	6.57	85
5	0.65	60000	0.60	80240	1	0.8319	0	8.33	90
6	0.65	60000	0.64	59196	4	0.4016	0.2008	6.90	90
7	0.54	73000	0.49	82585	1	0.5889	0	7.89	88
8	0.54	73000	0.54	86147	4	0.3160	0.1293	7.07	88

the number-average molecular weights were selected in order to force the use of very different amounts of initiator in the different batches. To avoid experiments that lasted too long, the desired weight-average molecular weights were smaller for higher monomer conversions. Table III shows the theoretical (desired) values and the experimental values obtained for monomer conversion, number-average molecular weight, batch time, and amount of initiator that should be added at the reaction start-up and at the beginning of each time interval.

Experimental runs 1 and 2 were performed in order to evaluate the performance of the controller for different final reactor conditions. It can be seen that good results were achieved, showing that the control technique could be used efficiently. The experiments in Table III also show that the absence of feedback information may lead to significant deviations between the desired values for monomer conversion and number-average molecular weight and the actual values obtained (Experiments 4–8). Analyzing the other results of Table III, it can be observed that the increase in the number of intervals (N) led to a decrease in the total time of the batch run. The larger the desired conversion, the larger was the reduction in the batch time.

It should be remembered that the states corresponding to the molecular weight distribution cannot be observed directly from measurements of concentrations of the constituents of the reaction system. As considerable time delay may be necessary to do GPC measurements, the strategy of Schuler and Zhang[38] was adopted, according to which, the states of the molecular weight distribution are not directly estimated; instead, the states corresponding to the concentrations of the reaction mixture components are estimated, and these values are used for estimating the molecular weight distribution, using the Kalman filter.

Figures 8 and 9 show the evolution of the monomer conversion and average molecular weights along experimental runs 7 and 8, respectively. It can be clearly seen that there was excellent agreement between the Kalman filter estimations and the experimental results in all cases. If the imperfect character of the model and the approximately 10% error rate of GPC analysis are taken into account, the performance of the Kalman filter can be regarded as excellent. Using the combination of NIR spectroscopy and the Kalman filter provided reliable estimates of the reactor states for control purposes.

Model predictive control

To evaluate the feasibility of using NIR spectroscopy for polymerization reactor monitoring and control, another process control strategy was examined. Because of its economical character and the reported number of applications in which it is used, the model predictive control approach was chosen. Four experimental runs were carried out using this process control technique. The first two runs dealt with simultaneous control of monomer conversion and molecular weight averages through manipulation of the initiator feed. The last two runs regarded the control of monomer conversion through manipulation of the reaction system temperature. The desired set-point values for the final monomer conversion and number-average molecular weight and the experimental values obtained are presented in Table IV.

Experimental runs 9 and 10 involved manipulation of the initiator feed to control the monomer conversion and the number-average molecular weight simultaneously, while keeping the reactor temperature constant. Reaction 9 was similar to reactions 1, 5, and 6 (Table III). Reaction 10 was similar to reaction 2, shown in Table III.

The control actions were computed through minimization of the following objective function:

$$\min\left(\sum_{i=k}^{k+NH}\left[\frac{X_d(i)-X_{\text{model}}(i)}{X_{\text{final}}}\right]^2+\left[\frac{Mw_d(i)-Mw_{\text{model}}(i)}{Mw_{\text{final}}}\right]^2+\left[\frac{Mn_d(i)-Mn_{\text{model}}(i)}{Mn_{\text{final}}}\right]^2\right) \quad (41)$$

where the set-point reference values X_d, Mw_d, and Mn_d are assumed to be the optimal control profiles, com-

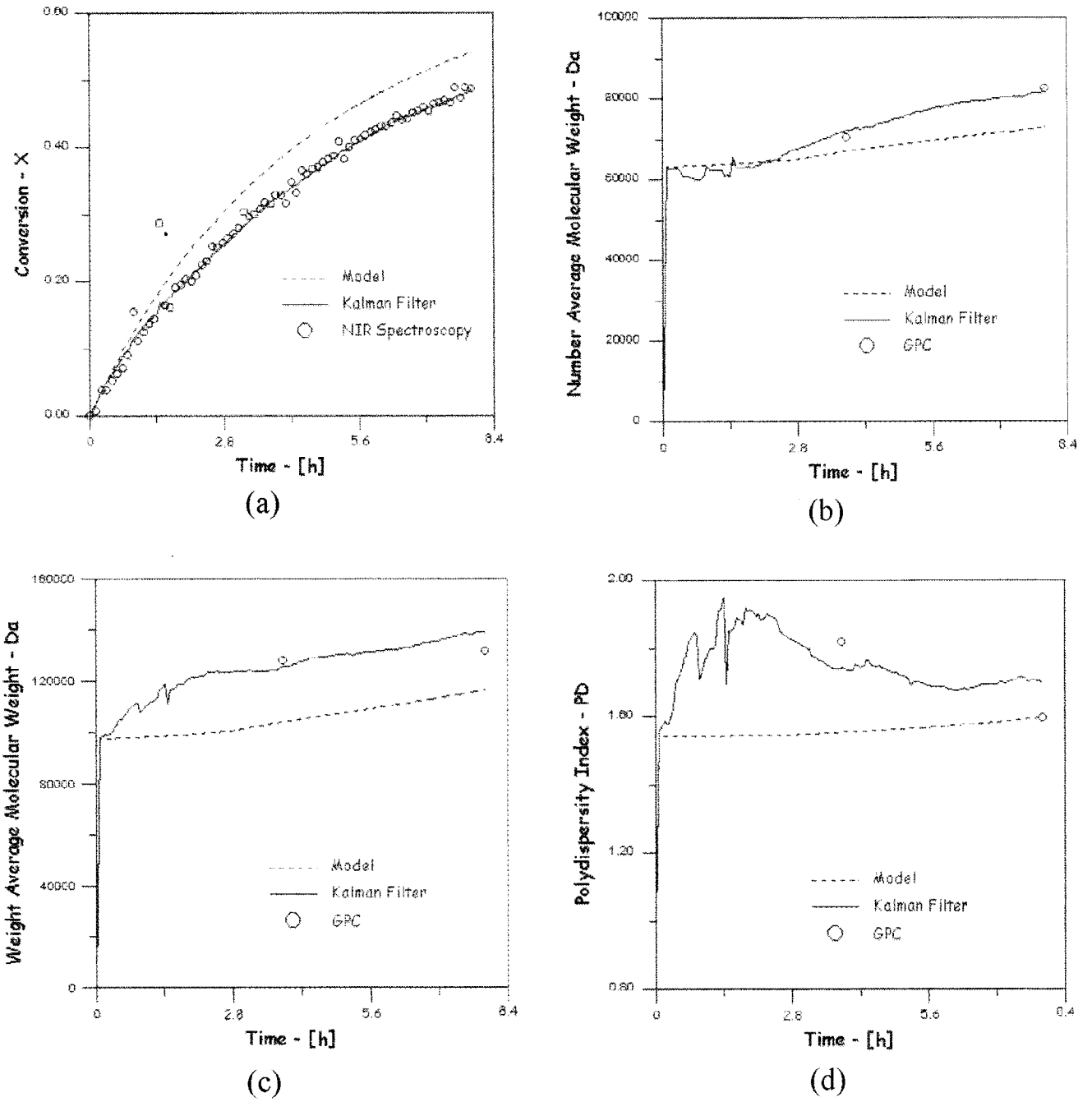

Figure 8 For experimental run 7: (a) evolution of monomer conversion, (b) number-average molecular weight, (c) weight-average molecular weight, and (d) polydispersity index.

puted as described previously for $N = 1$; and X_{model}, Mw_{model}, and Mn_{model} are the model predictions obtained with the Kalman filter, with states updated by NIR spectrophotometry and the reactor thermocouple. The sampling time was 10 min and the control horizon, NH, was computed as the number of 10-min segments required to reach the specified batch time. Depending on the particular experiment being considered, either the initiator load or the reactor temperature at interval t_i was manipulated to minimize the objective function. Finally, X_f, Mn_f, and Mw_f were included in the objective function in order to normalize the importance of the observed deviations.

In all cases, the initial load of initiator used experimentally was very different from the optimum values computed with the help of the optimum control algorithm. This was intentional, done to force the controller to modify the optimum initiator feed policies in order to follow the ideal optimum trajectory. Both the optimum and experimental initial loads of the initiator are presented in Table IV.

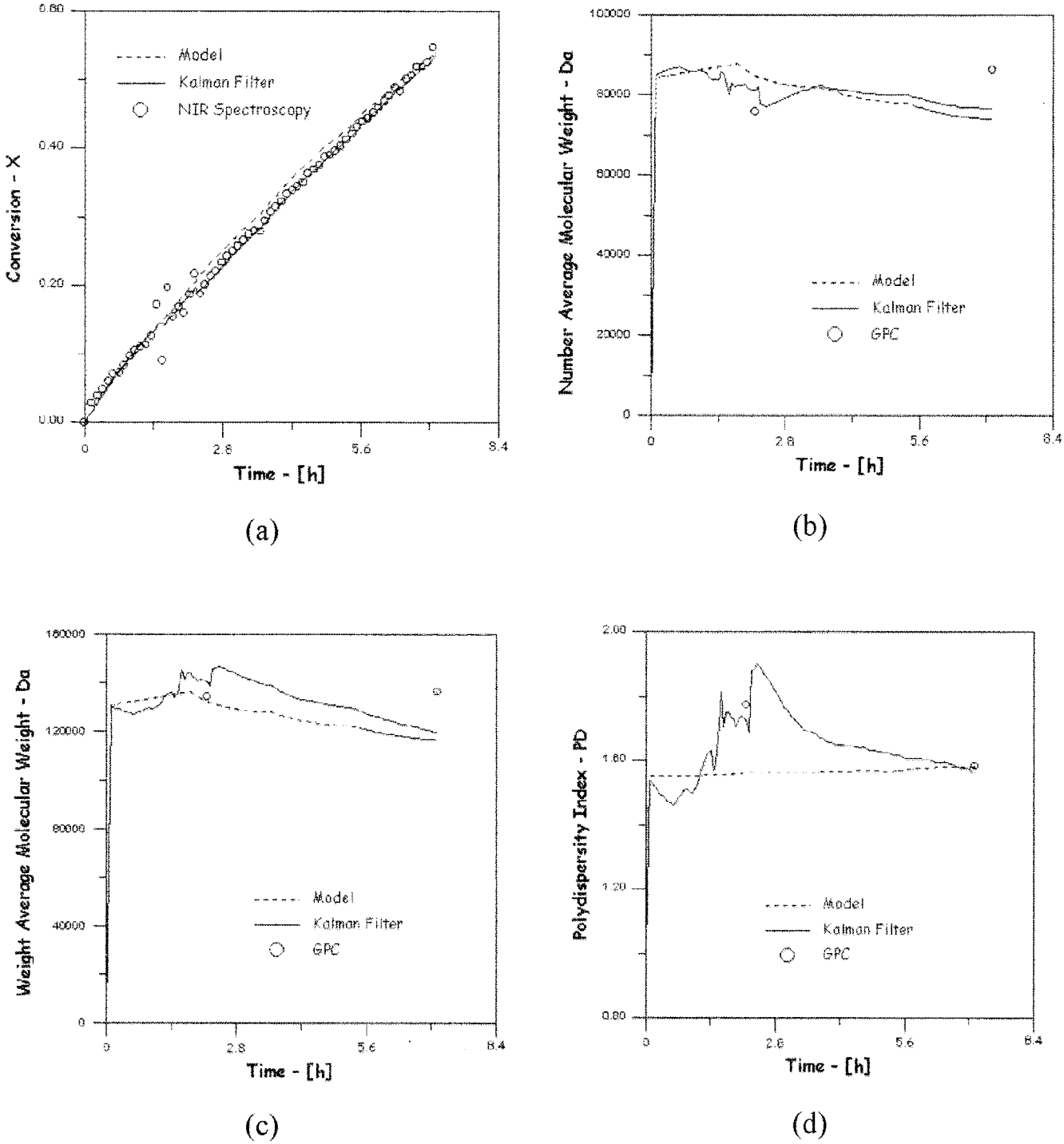

Figure 9 For experimental run 8: (a) evolution of monomer conversion, (b) number-average molecular weight, (c) weight-average molecular weight, and (d) polydispersity index.

Figure 10 shows the evolution of the monomer conversion, molecular weight averages, and initiator feed policies for experimental run 10. To disturb the process and make the process control more difficult, about 20% of the optimum amount of initiator was initially loaded into the reactor. As a consequence, open-loop responses would lead to much lower monomer conversions and much higher average molecular weights. Despite the huge process perturbation, it can be seen that the control objectives were tracked very well. The Kalman filter detected that the polymer concentration was too low and that the average polymer weight was too high compared to the desired optimum trajectories and that the amount of initiator should be increased. When the optimum initiator feed rates were reoptimized in-line, based on the states

TABLE IV
Set-Point Values and Experimental Results of Model Predictive Control Technique

Exp.	X_d	M_{n_d}	X_{exp}	$M_{n_{\text{exp}}}$	$[I_0] \cdot 10^2$ (mol/L)	$[I_0] \cdot 10^2$ (mol/L) (nominal)	t_f − (h)	T − (°C)
9	0.64	58000	0.65	59784	0.1433	0.8527	7.60	91
10	0.78	28000	0.76	38148	0.1433	3.8660	6.67	80
11	0.55	—	0.55	29151	4.6081	0.6998	6.67	—
12	0.81	—	0.81	45507	2.3040	8.3479	7.00	—

provided by the Kalman filter, a large amount of initiator had to be added to the reactor, as can be seen in Figure 10(d). Figure 10(a–c) shows that the controller provoked a remarkable change in the dynamic trajectories and led the system to approach the desired set-point values very closely.

The reactor temperature was also used as the main manipulated variable for controlling monomer conversion in runs 11 and 12, shown in Table IV. In this case the control of the final average molecular weight was not sought. There were two main reasons for this: first, because the temperature profile exerts a relatively small effect on the final average molecular weights of the polymer in the range of operation conditions analyzed in this study; and second, to illustrate how important the NIRS/Kalman filter feedback signal is for the proper and accurate control of the reaction course. Therefore, in experiments 11 and 12 the objective function to be minimized was formed by the summation of the square of the difference between the desired and the experimental (NIR spectroscopy) monomer conversion values. During optimization the temperature was constrained to the interval 60°C–90°C in order to satisfy actual system safety and operation constraints.

Figure 11 shows the evolution of the monomer conversion, the average molecular weights, and the manipulated temperature profiles for experimental run 12. It can be observed that the controller tracked the monomer conversion profile very accurately, as might already be expected. As the average molecular weights were not included in the objective function, controller responses did not attempt to track the set-point profiles desired for the molecular weights. For this reason, set-point values and experimental molecular weight data are very different. Despite that, model simulations indicate that model and filter predictions were in very good agreement. This shows again that the NIRS/Kalman filter monitoring strategy was able to estimate the actual system states properly.

Simultaneous control of monomer conversion and polymer average molecular weight through simultaneous manipulation of the reactor temperature and initiator feed rates was also performed by simulation, but the results obtained were similar to the ones already presented in Figures 9–10. Therefore, these experiments were not performed because they would not add any significant information about the feasibility of using NIRS as an alternative technique for the monitoring and control of solution polymerization reactions.

CONCLUSIONS

NIR spectroscopy was used to monitor and control a styrene solution polymerization reactor, with the help of a Kalman filter estimator. The results of experiments and simulations clearly showed that NIRS can be used very successfully for in-line and *in situ* monitoring of monomer conversion and polymer average molecular weight, using a simple and accurate combination of a calibration model and a first-principle process model.

The first-principle model of the solution polymerization process was used as a basis for the design of two process control strategies, one based on the optimal control theory while the other based on the well-known model predictive control. These control strategies were then used to evaluate whether the process control loop could be successfully closed with the in-line information provided by the NIR spectroscopy, with the help of the Kalman filter estimator. Using these techniques and NIR spectroscopy, it was shown both theoretically and experimentally that NIR spectroscopy could be used very successfully for in-line process control applications. In particular, the combination of NIRS and the Kalman filter allowed the simultaneous control of monomer conversion and polymer average molecular weights through manipulation of initiator feed rates and reactor temperature.

NOTATION

$A_{\lambda = 1207\ \text{nm}}$	value of second derivative absorbance of NIR spectra at $\lambda = 1207$ nm
$[b_i]$	initiator concentration at the beginning of interval i (mol/L)
e	model predictive control error function
Exp	number of the experimental run
F	Jacobian matrix of **f**

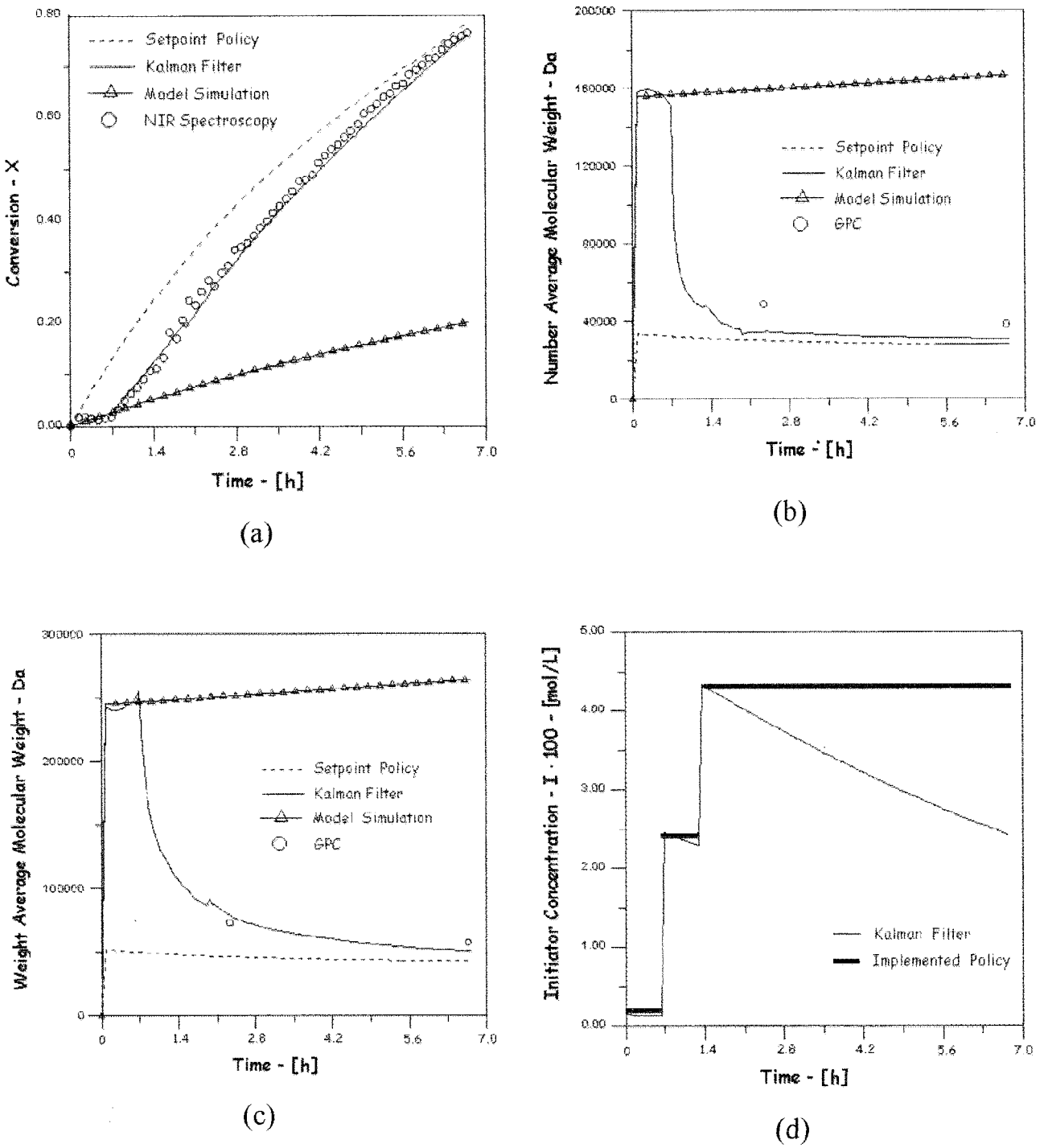

Figure 10 For experimental run 10: (a) evolution of monomer conversion, (b) number-average molecular weight, (c) weight-average molecular weight, and (d) initiator concentration profile.

f	vector of the process model equations	I	identity matrix [(eq. (34)]
f	initiator efficiency	I	initiator concentration (mol/L)]
g	gel effect correction factor	$[I]_0$	initiator concentration at reactor start-up (mol/L)
H_k	Jacobian matrix of $\mathbf{h_k}$	k	sampling instant
h	vector of system output functions	k_d	kinetic constant of initiator decomposition (s^{-1})
h_k	vector of system output functions calculated at sampling instant k	K_k	filter gain calculated at sampling instant k
i	sampling instant in model predictive control		

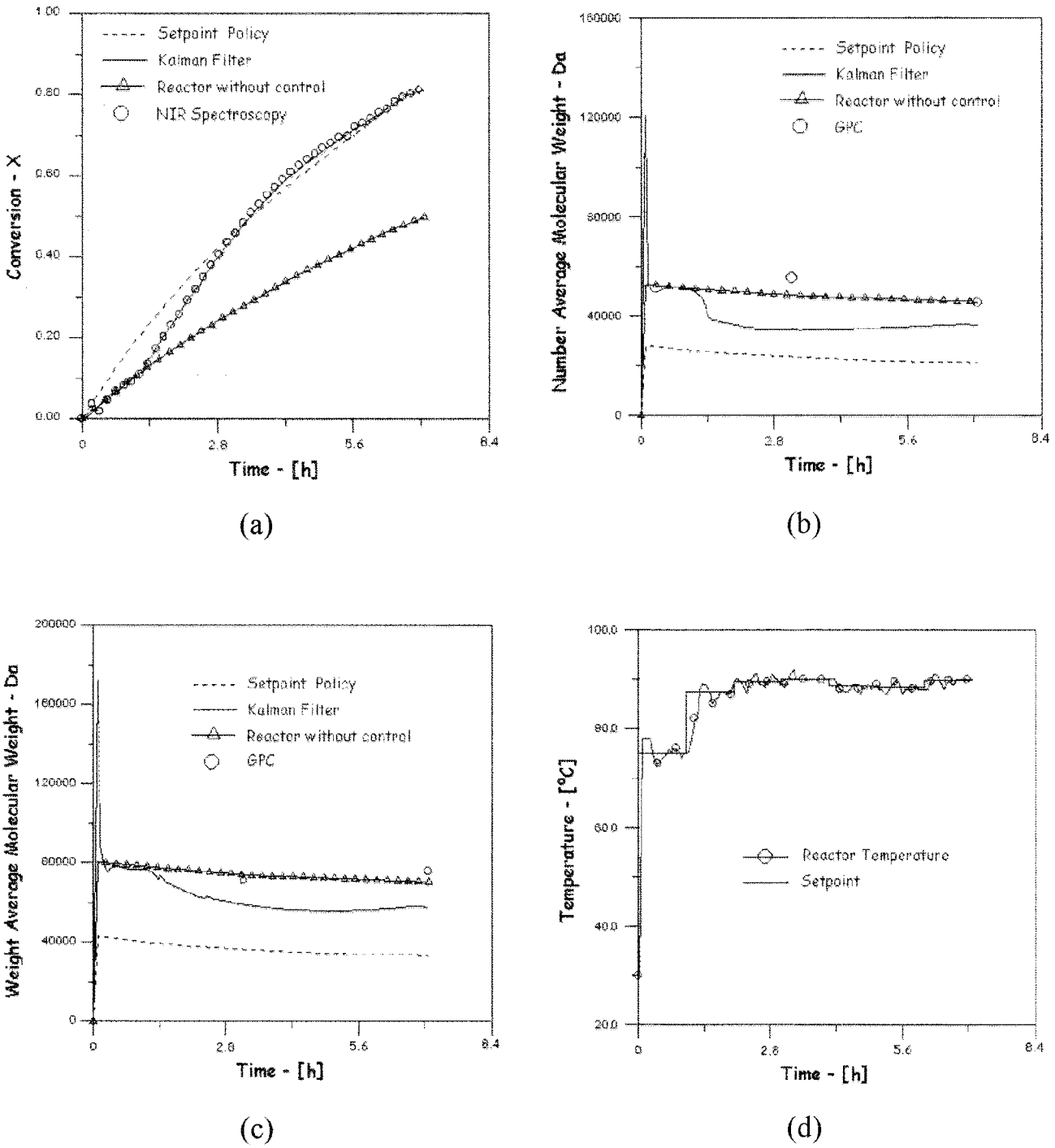

Figure 11 For experimental run 12: (a) evolution of monomer conversion, (b) number-average molecular weight, (c) weight-average molecular weight, and (d) temperature profile.

k_p kinetic constant of the propagation reaction (L mol^{-1} s^{-1})

k_{fm} kinetic constant of the chain transfer to monomer reaction (L mol^{-1} s^{-1})

k_{fs} kinetic constant of the chain transfer to solvent reaction (L mol^{-1} s^{-1})

k_{tc} kinetic constant of the termination reaction by combination (L mol^{-1} s)

k_{tc0} kinetic constant of the termination reaction by combination at 0% of monomer conversion (L mol^{-1} s^{-1})

m chain length

M model predictive control horizon

M monomer concentration (mol/L)

M_0 monomer concentration at reactor start-up (mol/L)

M_n number-average molecular weight (Da)
$M_{n\,d}$ number average molecular weight desired at end of experimental run (Da)
$M_{n\,exp}$ experimental number-average molecular weight obtained at end of experimental run (Da)
$M_{n\,f}$ number-average molecular weight of final product (Da)
$M_{n\,model}$ number-average molecular weight predicted by model (Da)
M_w weight-average molecular weight (Da)
$M_{w\,f}$ weight-average molecular weight of final product (Da)
$M_{w\,model}$ weight-average molecular weight predicted by model (Da)
N number of intervals into which total batch time divided
NH control horizon of model predictive control objective function
n chain length
$P_k(+)$ error covariance matrix after being updated
$P_k(-)$ error covariance matrix before being updated
P prediction horizon
PM_{monomer} molecular weight of the monomer (g/gmol)
P_n growing radical with chain length equal to n
PSt weight percent of polystyrene present in reaction media
R universal gas constant (cal $\text{mol}^{-1} \cdot \text{K}^{-1}$)
R_W covariance of the Gaussian noise of system states measurements
R_V covariance of the Gaussian noise of system output measurements
R· radical formed by decomposition of initiator
R^2 Correlation coefficient
S Solvent concentration (mol/L)
t time (s)
t_f total time of batch (s)
T temperature (K or °C)
u vector of control actions
$u_{\max}$ vector with maximal possible values for control actions
$u_{\min}$ vector with the minimal possible value for control actions
V reaction mixture volume (L)
V_{m0} volume of monomer at reactor startup (L)
V_S volume of solvent present in reaction mixture (L)
X monomer conversion
$\hat{\imath}(+)$ vector of system states after being updated
$\hat{\imath}(-)$ vector of system states before being updated
x vector of system states
X_d desired value of monomer conversion at end of experimental run
X_{exp} experimental value obtained for the monomer conversion at end of experimental run
X_f monomer conversion at end of batch
$x_{\max}$ vector with maximal possible values for system states
$x_{\min}$ vector with minimal possible values for system states
X_{model} monomer conversion predicted by the mathematical model of the
y vector of system outputs
$y_{\max}$ vector with maximal possible values for system outputs
$y_{\min}$ vector with minimal possible values for system outputs

Greek Symbols

θ_n dead polymer with chain length equal to n
Θ model predictive control objective function
α parameter of gel effect correction factor expression
β parameter of gel effect correction factor expression
γ parameter of gel effect correction factor expression
ϵ volume contraction factor
ρ_M density of monomer (g/mL)
ρ_S density of solvent (g/mL)
λ_k moment of order k of distribution of growing radicals
μ_k moment of order k of distribution of dead polymer chains
$\Delta u_{\max}$ maximum variation allowed for control action

References

1. Ogunnaike, B. A. Annu Rev Control 1996, 20, 1.
2. Seborg, D. E. European Control Conference, August 1999; p 1–32.
3. Embiruçu, M.; Lima, E. L.; Pinto, J. C. Polym Eng Sci 1996, 36, 433.
4. Kiparissides, C. Chem Eng Sci 1996, 51, 1637.
5. Vega, M. P.; Lima, E. L.; Pinto, J. C. Comput Chem Eng 1997, 21, S1049.
6. Pinto, J. C.; Ray, W. H. Chem Eng Sci 1995, 50, 1041.
7. Odian, G. Principles of Polymerization, 3rd ed.; John Wiley: New York, 1991.
8. Ellis, M. F.; Taylor, T. W.; Jensen, K. F. AIChE J 1994, 40, 445.
9. Crowley, T. J.; Choi, K. Y. Chem Eng Sci 1998, 53, 2769.
10. Zaldívar, C.; Iglesias, G.; Del Sol, O.; Pinto, J. C. Polymer 1997, 383, 5823.
11. Zaldívar, C.; Del Sol, O.; Iglesias, G. D. Polymer 1997, 39, 245.
12. Giudici, R. Latin American Appl Res 2000, 30, 351.

13. Chien, D. C. H.; Penlidis, A. J Macromolecular Sci—Rev Macromolecular Chem Phys 1990, C30(1), 1.
14. Kammona, O.; Chatzi, E. G.; Kiparissides, C. J Macromolecular Sci—Rev Macromolecular Chem Phys 1990, C39(1), 57.
15. Santos, A. F.; Lima, E. L.; Pinto, J. C. J Appl Polym Sci 1998, 70, 1737.
16. Santos, A. F.; Lima, E. L.; Pinto, J. C. J Appl Polym Sci 2000, 77, 453.
17. Vieira, R. A. M.; Sayer, C.; Lima, E. L.; Pinto, J. C. Ind Eng Chem Res 2002, 41, 2915.
18. Long, T. E.; Liu, H. Y.; Schell, B. A.; Teegarden, D. M.; Uerz, D. S. Macromolecules 1993, 26, 6237.
19. DeThomas, F. A.; Hall, J. W.; Monfre, E. S. L. Talanta 1994, 41, 425.
20. Cherfi, A.; Fevotte, G. Macromolecular Chem Phys 2002, 203, 1188.
21. Cherfi, A.; Fevotte, G. Novat, C. J Appl Polym Sci 2002, 85, 2510.
22. Ray, W. H. J Macromol Sci—Rev Macromol Chem 1972, C8(1), 1.
23. Levenspiel, O. Chemical Reaction Engineering, 2nd ed.; John Wiley: New York, 1972.
24. Chen, S. A.; Huang, N. W. Chem Eng Sci 1981, 36, 1295.
25. Fontoura, J. M. R. M.Sc. Thesis, Universidade Federal do Rio de Janeiro/COPPE, Rio de Janeiro, 1996 (in Portuguese).
26. Sargent, R. W. H. J Comput Appl Math 2000, 124, 361.
27. Hsu, K. Y.; Chen, S. A. Chem Eng Sci 1988, 43, 1311.
28. Morari, M.; Lee, J. H. Comput Chem Eng 1999, 23, 667.
29. Soroush, M. Comput Chem Eng 1998, 23, 229.
30. Kozub, D. J.; MacGregor, J. F. Chem Eng Sci 1992, 47, 1047.
31. van Dootingh, M.; Viel, F.; Rakotopara, D.; Gauthier, J. P.; Hobbes, P. Comput Chem Eng 1992, 16, 777.
32. Neitzel, I.; Lenzi, M. K. Comput Appl Eng Ed 2001, 9(2), 101.
33. Bishop, R. H. Learning with LabView, 1st ed.; Addison-Wesley: Palo Alto, CA, 1999.
34. NIRSystems. NIRSystems Process Analytics Manual, Version 1.0; NIRSystems: Silver Springs, MD, 1994.
35. Wold, S.; Sjöström, M. Chemometrics and Intelligent Laboratory Systems 1998, 44, 3.
36. Sonnessa, A. J. Introduction to Molecular Spectroscopy, 1st ed.; Reinhold Publishing: New York, 1966.
37. Siesler, H. W. Makromol Chem, Macromol Symp 1991, 52, 113.
38. Schuler, H.; Zhang, S. H. Chem Eng Sci 1985, 40, 1891.
39. Brandrup, J.; Immergat, E. H. Polymer Handbook, 2nd ed.; John Wiley & Sons: New York, 1975.
40. Stevens, C. J. Mathematical Modeling of Bulk and Solution Free-Radical Polymerization in Tabular Reactors; Ph.D. Thesis; University of Wisconsin, Madison, 1988.
41. Swern, D. Organic Peroxides 1st ed.; John Wiley & Sons: New York, 1970.
42. Perry, R. H.; Green, D. W. Perry's Chemical Engineers' Handbook, 7th ed. McGraw-Hill, 1997.